Journal of Molecular Structure 1275 (2023) 134618

Contents lists available at ScienceDirect

Journal of Molecular Structure

journal homepage: www.elsevier.com/locate/molstr

Prunus mahaleb shell as a sustainable bioresource for carminic acid removal from aqueous solution: Experimental and theoretical studies

Zehra Seba Keskin[a,*], Zeynep Mine Şenol[b], Savaş Kaya[a], Selçuk Şimşek[c]

[a] Department of Pharmacy, Cumhuriyet University, Health Services Vocational School, Sivas 58140, Turkey
[b] Department of Food Technology, Cumhuriyet University, Zara Vocational School, Sivas 58140, Turkey
[c] Department of Chemistry, Sivas Cumhuriyet University, Sivas 58140, Turkey

ARTICLE INFO

Article history:
Received 9 September 2022
Revised 12 November 2022
Accepted 21 November 2022
Available online 25 November 2022

Keywords:
Bioresource
Prunus mahaleb shell
Carminic acid
Wastewater treatment

ABSTRACT

This study focused on the performance of *Prunus mahaleb* shell (MS) agricultural waste, which is used as an alternative biosorbent for carminic acid (CA) removal from aqueous solution. The effects of different parameters such as pH, initial dye concentration, contact time, biosorbent dosage and temperature on the biosorption of CA dye to the MS biosorbent surface were investigated. The characterization of the biosorbent was done by FT-IR, SEM-EDX and pzc analyses. It was determined that the isotherm and kinetics of CA dye removal were consistent with the Langmuir isotherm and PSO and IPD kinetic models, respectively. The maximum adsorption capacity was calculated as 148 mg g^{-1} according to the Langmuir isotherm. According to the ΔH^0, ΔG^0 and ΔS^0 results, the biosorption was found to be endothermic and spontaneous. Based on these data, it is concluded that environmentally friendly, inexpensive, simple to use and effective MS biosorbent can be used for CA dye removal.

© 2022 Elsevier B.V. All rights reserved.

1. Introduction

With the increase in population and the development of industries in recent years, the primary concern worldwide has been the maintenance of adequate and good water quality [1]. Colored dyes are among the main pollutants that cause water pollution in many industries such as paint manufacturing, textile, paper, food, leather, cosmetics and plastics [2]. Many dyes are toxic and are not biodegradable. Discharge of these dyes into waste water negatively affects vital activities such as drinking, washing and bathing [3]. They can also cause dysfunction in the brain and central nervous system, liver, kidneys, reproductive system, and cancer [4]. They can affect photosynthetic activity as they reduce sunlight transmission and can be toxic to aquatic life due to metals and aromatics [5].

Carminic acid (E120) is an anionic and anthraquinone-based organic food dye obtained from the cochineal bugs [6,7]. It is widely used in textile, cosmetics, printing, food industry, medical and pharmaceutical applications [8]. According to the World Health Organization (WHO), CA is considered safe at low concentrations of 0.005 mg L^{-1}. However, it is a toxic and neurotoxic dye that can cause skin and eye diseases and cancer in higher intakes [9].

For these reasons, suitable techniques for the effective removal of dyes are investigated before the discharge of industrial wastewater. Many techniques such as coagulation, chemical oxidation, membrane separation, and electrochemical, aerobic, and anaerobic microbial degradation are applied to treat dye-containing wastewater. However, these methods are not widely used due to many disadvantages [10]. Among all these methods, adsorption is preferred more than other techniques because of its low cost, flexible and simple design, resistance to toxic substances, and high efficiency [11]. Among the factors affecting the adsorption efficiency, adsorbent-adsorbate interaction, adsorbent surface, adsorbent surface area, adsorbate/adsorbent ratio, and adsorbent particle size, temperature and pH are extremely important [12]. For this reason, in many studies, the applicability of using renewable, cheap, and abundant agricultural wastes as adsorbents has been reported compared to other adsorbent types [13–15].

Prunus mahaleb L. belongs to the *Prunoidae* subfamily of the Rosaceae family. *Prunus mahaleb* is a species that can adapt well to marginal soils, with an average tree length of 1–5 m, and sheds its leaves in winter. Mahaleb fruit, which grows abundantly in the centers of Europe and Asia and in the regions of North Africa, is consumed both fresh and in powder form. While it is used in the food industry with its bitter taste and intense aroma, it is preferred in the health and pharmaceutical industry due to the heart-protective, antidiabetic, antifungal, and cytotoxic properties of anthocyanins, coumarins, flavonols, and fatty acids. It is also among the important export products for Turkey [16,17].

* Corresponding author.
E-mail address: zkeskin@cumhuriyet.edu.tr (Z.S. Keskin).

https://doi.org/10.1016/j.molstruc.2022.134618
0022-2860/© 2022 Elsevier B.V. All rights reserved.

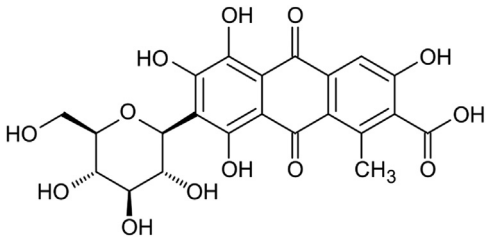

Fig. 1. Chemical structure of Carminic acid dye.

The aim of this study is to determine the adsorption capacity and optimum conditions of CA from aqueous medium to the surface of *Prunus mahaleb* shell (MS). The reason for choosing MS as an biosorbent is that, as far as we know, and according to the literature review, it has not been used in any study. It is also in a lignocellulosic structure and can be found in abundance. The study was carried out in a batch system using different parameters such as contact time, pH effect, adsorbent dosage, dye initial concentration, and temperature. In order to understand the biosorption process, adsorption equilibrium, kinetic and thermodynamic studies were carried out. The characterization of the biosorbent before and after adsorption was performed by FT-IR, SEM-EDX, and point of zero charge (pH_{pzc}) analyses.

2. Materials and method

2.1. Materials

CA is a red food additive known as E 120. 7-β-D-gluco pyranosyl-3,5,6,8-tetrahydroxy-1-methyl 9,10-dioxoanthracene-2-carboxylic acid (Fig. 1) with a molecular weight of 492.39 g mol^{-1} and a molecular formula of $C_{22}H_{20}O_{13}$ is an anthraquinone colorant [18]. MS biosorbent was obtained from a regional factory in Niksar, Tokat, Turkey. All chemicals used are of analytical purity. All experiments were done with double deionized water.

2.2. Characterization

Equilibrium solution concentrations of CA dye were measured by Shimadzu 160A, UV–vis spectrophotometer. The functional groups in the MS biosorbent before and after biosorption were determined by Fourier Transform Infrared (FT-IR) analysis. FT-IR analysis was performed in the 400–4000 cm^{-1} range using Bruker Model: Tensor II. The surface morphology of the samples was observed with an energy dispersive spectrophotometer-assisted (SEM-EDX) Tescan MIRA 3 XMU scanning electron microscope. Selecta pH meter with a glass-calomel electrode was used for pH adjustments and pHpzc determination. Nuve NT12 thermostatic water bath was used in thermodynamic studies.

2.3. Batch biosorption procedure

The biosorption of CA dye onto the MS biosorbent was investigated using the batch method. Biosorption experiments were carried out by adding 100 mg biosorbent to dye solutions with 500 mg L^{-1} constant concentration and 10 mL volume at ambient pH:8.9 for 24 h in propylene tubes. The removal of CA dye (Removal%) and the concentration of CA dye biosorbed during the equilibrium time (Q, mol kg^{-1}) are given in Eqs. (1) and (2).

$$Removal\% = \left(\frac{C_O - C_e}{C_O}\right) X 100 \quad (1)$$

$$Q = (C_o - C_e).V/m \quad (2)$$

where, C_0 (mg L^{-1}) represents the initial dye concentration, C_e (mg L^{-1}) represents the dye concentration at equilibrium time (mg L^{-1}), m (mg) biosorbent amount, and V (L) solution volume.

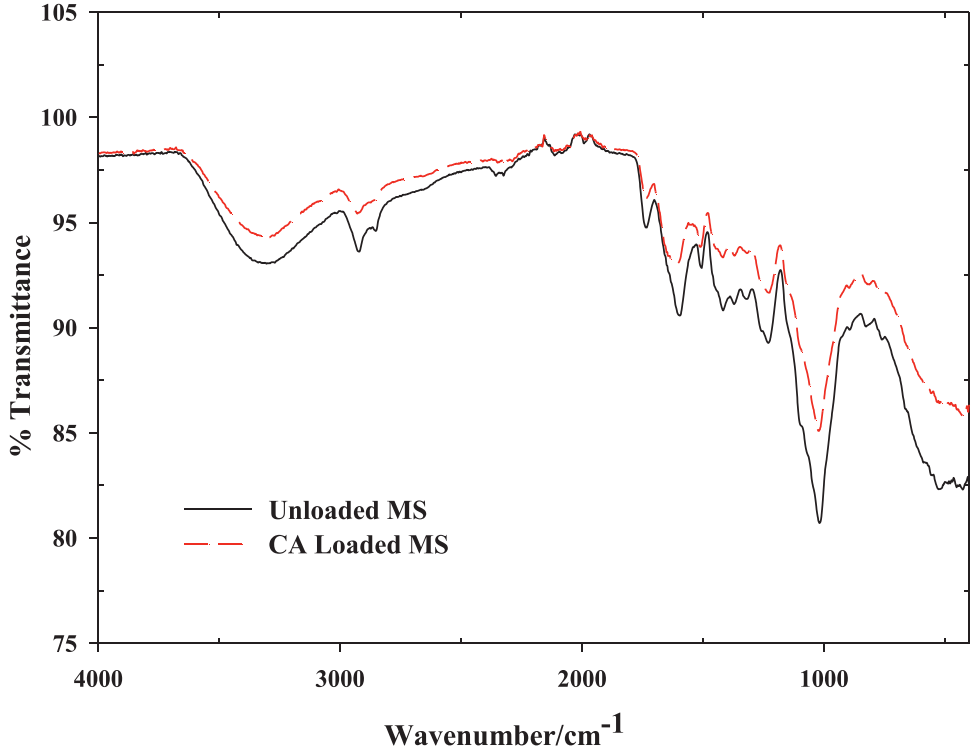

Fig. 2. FT-IR spectra of unloaded and CA loaded MS biosorbent {$[CA]_0$: 500 mg L^{-1}, biosorbent dosage: 100 mg, V: 10 mL, natural pH: 8.9, contact time: 24 h, temperature: 25 °C}.

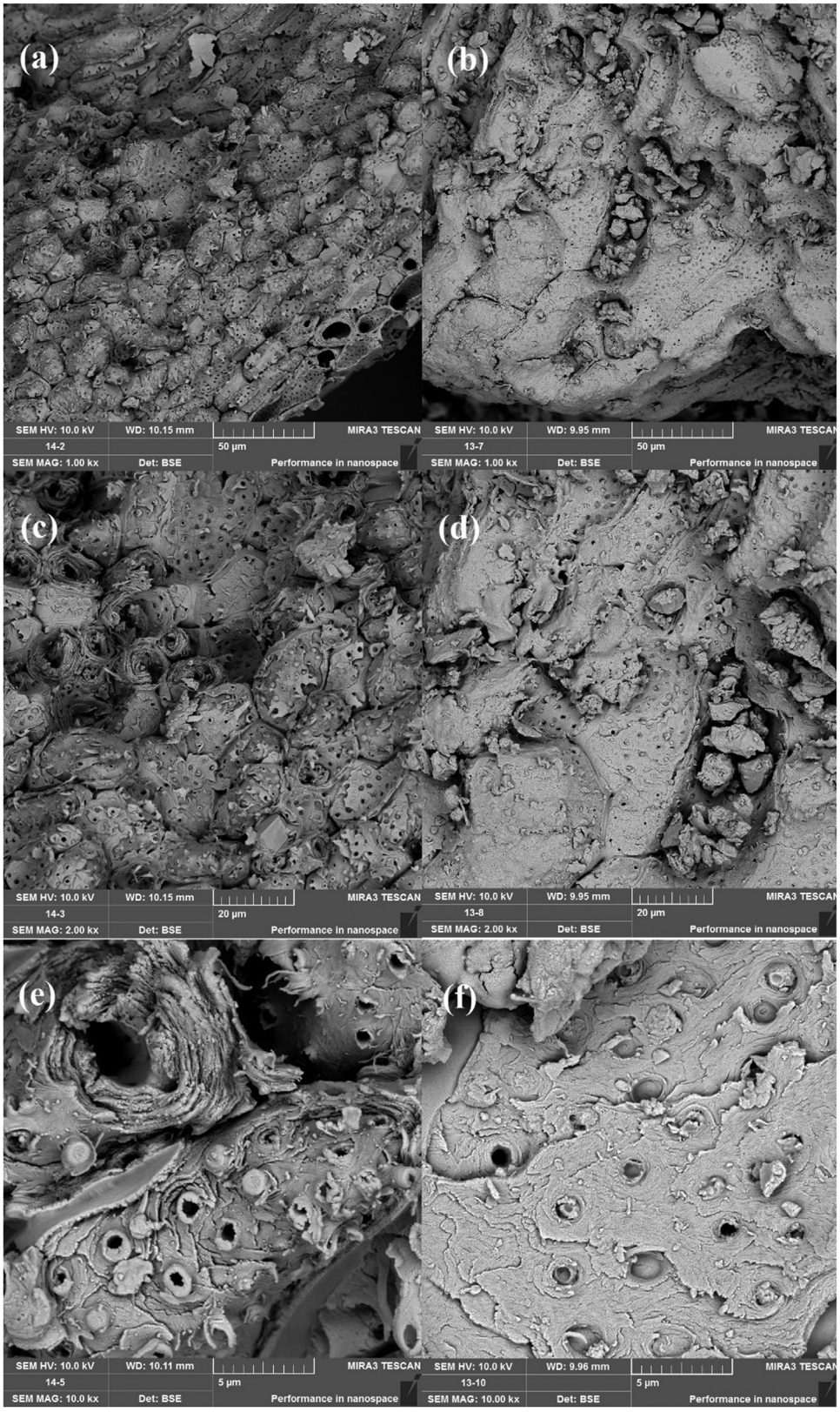

Fig. 3. SEM photographs of MS biosorbent before (a, c, e) and after (b, d, f) biosorption of CA {$[CA]_0$: 500 mg L^{-1}, biosorbent dosage: 100 mg, V: 10 mL, natural pH: 8.9, contact time: 24 h, temperature: 25 °C}.

2.4. Recovery procedure

HCl, ethanol and methanol solutions (0,1 mol L^{-1}) were used to recover CA dye from the MS biosorbent surface. For the biosorption/desorption cycle, the experiments were repeated 5 times and at the end of the experiment, the solutions were centrifuged for liquid-solid separation. The amount of CA dye in the obtained equilibrium solution was determined by reading at 504 nm in a UV–vis spectrophotometer. Recovery% was calculated using the following Eq. (3).

$$\text{Recovery\%} = \frac{Q_{des}}{Q_{ads}} x100 \quad (3)$$

Q_{des} in the equation; the amount of CA recovered (mg g^{-1}), Q_{ads}; represents the amount of biosorbed CA (mg g^{-1}).

3. Results and discussion

3.1. FT-IR results

FT-IR spectroscopy provides information about functional groups on the MS surface that provide active sites for CA dye biosorption. The FT-IR spectrum for before and after biosorption is shown in Fig. 2. The strong and wide band observed between 3672 cm^{-1} and 3000 cm^{-1} can be associated with the O–H stretching vibration of phenolic, alcoholic, and carboxylic functional groups [19]. The peaks observed at 2926 cm^{-1} and 2850 cm^{-1} can be attributed to the C–H stretching of the -CH_3 and CH_2 groups [20]. The peak at 1745 cm^{-1} shows the specific peak of C = O found in hemicellulose [21], while the peaks at 1600 cm^{-1} and 1500 cm^{-1} originate from the C = C aromatic groups in lignin [22]. The strong peak observed at 1021 cm^{-1} corresponds to the symmetrical or asymmetric vibration of the C–O-C, C–O and C–OH groups of cellulose [23].

After the biosorption of CA, significant decreases are observed in the intensity of the peaks observed in the FT-IR spectrum of MS biosorbent. This shows that there is an interaction between the functional groups of MS biosorbent and CA dye.

3.2. SEM-EDX results

SEM analysis technique was used to observe the morphological differences of MS biosorbent before and after the biosorption of CA. SEM images in Fig. 3(a, c, e) show the structure of MS before biosorption and Fig. 3(b, d, f) shows the structure after biosorption. Fig. 3(a, c, e) shows that the structure of the biosorbent is porous and irregular. In the SEM images in Fig. 3(b, d, f), it is clearly observed that after the biosorption, the pores turn into a smoother and more regular structure as they are filled with CA dye molecules. This significant differentiation in the structure of the biosorbent indicates surface complexation.

Elements before and after biosorption on MS were determined using EDX analysis and EDX spectra are given in Fig. 4. The peaks of C, N, and O were determined in the EDX analysis of MS before biosorption. After biosorption, since CA is an organic dye, peaks belonging to the same elements were observed in the EDX spectrum. The Al (0.35%) peak is thought to originate from the alum used during the processing of the CA dye.

3.4. Effect of pH on biosorption and determination of pH_{pzc}

Solution pH is one of the most important parameters affecting biosorbent surface properties, ionization of adsorbate material, and adsorption capacity. In this study, analyzes were carried out to determine the effect of solution pH on the biosorption of CA on the MS biosorbent surface, with an initial concentration of 500 mg L^{-1},

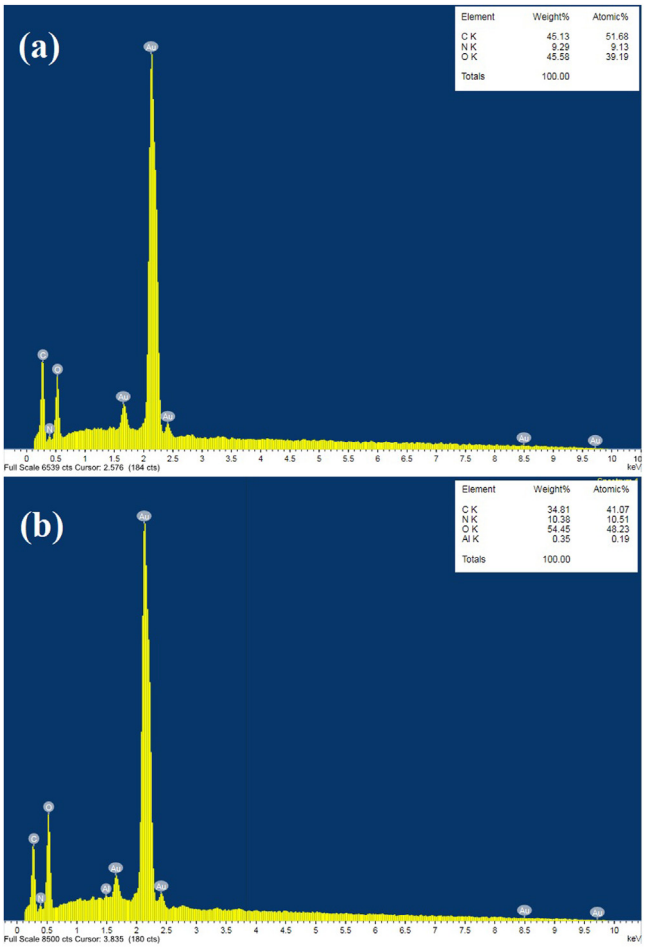

Fig. 4. EDX spectrum of MS biosorbent before (a) and after (b) biosorption of CA {$[CA]_0$: 500 mg L^{-1}, biosorbent dosage: 100 mg, V: 10 mL, natural pH: 8.9, contact time:24 h, temperature: 25 °C}.

a biosorbent dose of 100 mg, a contact time of 24 h and a pH range of 2–12. Fig. 5. showed the pH effect of the solution on the biosorption capacity of CA dye on the MS biosorbent. As seen in Fig. 5, there was no significant change in biosorption with the change in pH. After pH 8, it is seen that the biosorption capacity decreases.

In addition, the pH_{pzc} value of the biosorbent was determined as 5.24. While the biosorbent surface became negatively charged in the pH > pH_{pzc} condition, the biosorbent surface became positive in the pH < pH_{pzc} condition [24]. At pH values lower than the pH_{pzc}, the adsorption capacity increases due to increased electrostatic interactions between the positively charged biosorbent surface and anionic dye molecules such as CA dye. At pH values greater than the pH_{pzc}, solution OH^- ions and anionic dyes compete for binding to the active sites of the biosorbent. Thus, the biosorption capacity of the anionic dye decreases [25].

3.5. Biosorption isotherms

Biosorption isotherms help to explain the distribution of biosorption molecules and the biosorbent-adsorbate relationship in the liquid and solid phase when the biosorption process reaches equilibrium at constant temperature and pressure. In this study, the nonlinear equilibrium relationship between the concentration of CA dye biosorbed on MS biosorbent and the concentration of CA dye remaining in solution was investigated using Langmuir, Freundlich and Dubinin-Radushkevich (D-R) isotherm

Table 1
The biosorption isotherms and their parameters.

Isotherm models	Parameters	Value	
Langmuir	X_L: the maximum biosorption capacity	X_L (mg g^{-1})	148
$Q = \frac{X_L C_e}{1 + K_L C_e}$	K_L: the parameter for Langmuir isotherm	K_L (L mg^{-1})	1868
	Q: the amount of biosorbed CA	R^2	0.995
	C_e: the equilibrium concentration		
Freundlich	X_F: Freundlich constant	X_F	0.880
$Q = X_F C_e^{\beta}$	β: biosorbent surface heterogeneity	β	0.708
		R^2	0.991
$D - R$	X_{DR}: a measure of biosorption capacity	X_{DR} (mg g^{-1})	30410
$Q = X_{DR} e^{-(K_{DR}\varepsilon^2)}$	K_{DR}: the activity coefficient	$-K_{DR}x10^9/mol^2$ KJ^{-2}	0.209
$\varepsilon = RTln\left(1 + \frac{1}{C_e}\right)$	ε: the Polanyi potential		
	R:the ideal gas constant (8.314 $Jmol^{-1}K^{-1}$)	E_{DR}/kJ mol^{-1}	4.89
$E_{DR} = (2K_{DR})^{-0.5}$	E_{DR}: the biosorption energy	R^2	0.950
	T: the absolute temperature		

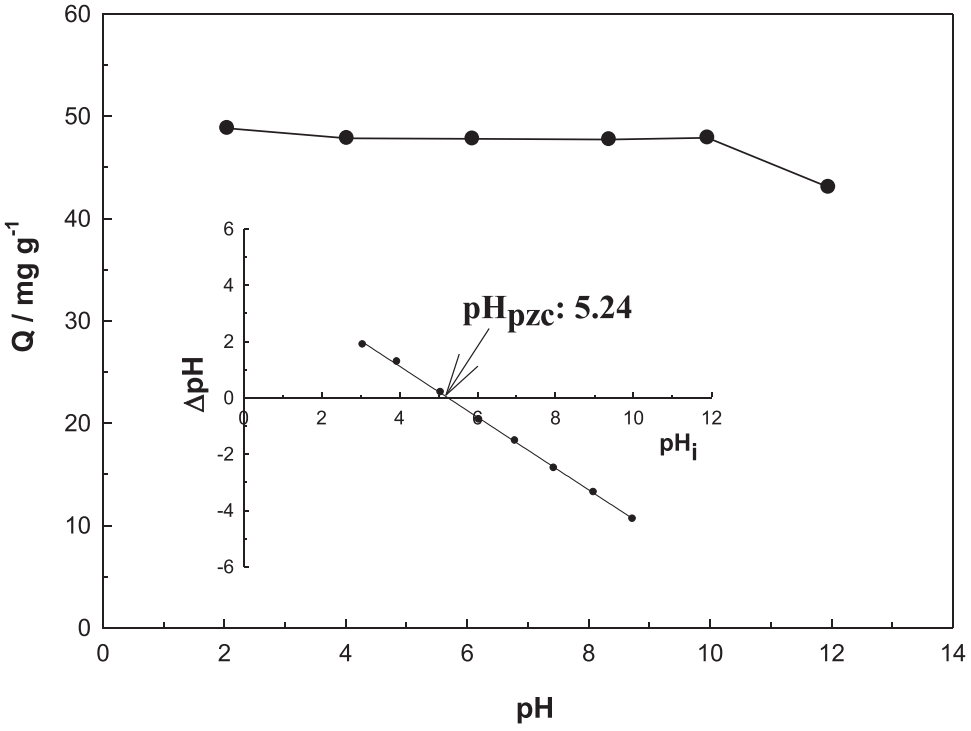

Fig. 5. Effect of pH on the biosorption of CA on MS biosorbent and pH_{pzc} for MS biosorbent {$[CA]_0$:500 mg L^{-1}, biosorbent dosage: 100 mg, V: 10 mL, pH: 2.0–12.0, contact time: 24 h, temperature: 25 °C}.

models. The Langmuir isotherm model assumes that the adsorbent surface is homogeneous and the number of active sites is constant. The maximum amount of biosorbed material is equal to the number of active centers on the biosorbent surface [31]. The Freundlich isotherm model assumes that the surface of the biosorbent is heterogeneous and multilayered and that the surface regions of the biosorbent have different binding energies [32]. The D-R isotherm model assumes that biosorption is related to surface porosity and pore volume, and examines biosorption energetically [33]. The mean free energy of biosorption (E_{DR}) obtained from the D-R model determines whether the adsorption structure is chemical or physical. 8< E_{DR} <16 kJ mol^{-1} indicates that the adsorption has a chemical character. If E_{DR} <8 kJ mol^{-1}, it determines that the adsorption is physical [34].

The isotherms determined for the biosorption of CA dye to the MS biosorbent are shown in Fig. 6. Langmuir, Freundlich and D-R isotherm equations and their derived parameters are presented in Table 1. When the nonlinear regression values of the Langmuir and Freundlich isotherm models were compared, it was determined that the Langmuir model (R^2: 0.995) was more appropriate to describe biosorption. This shows that the CA dye molecules bind to the active sites on the biosorbent surface as a monolayer. The maximum biosorbent capacity for the biosorbate was 148 mg g^{-1} and the K_L value was 1868 L mg^{-1}. The biosorption capacity measure obtained from the Freundlich isotherm model was found to be 0.880 and the surface heterogeneity to be 0.708. The E_{DR} of biosorption from the D-R model was calculated as 4.89 kJ mol^{-1}. This value shows that the CA dye biosorption process on the biosorbent is physically.

3.6. Biosorption kinetics

Parameters obtained by adsorption kinetic studies provide information about the determination of the adsorption rate, modeling of the adsorption process, and metal interactions between the adsorbate and the adsorbent [26]. Pseudo-first-order kinetic (PFO) model [27], pseudo-second-order kinetic (PSO) model [28] and intraparticle diffusion (IPD) models were applied to determine the adsorption kinetics of CA dye on the MS biosorbent surface [29]. The PFO model is used for reversible reactions in which an

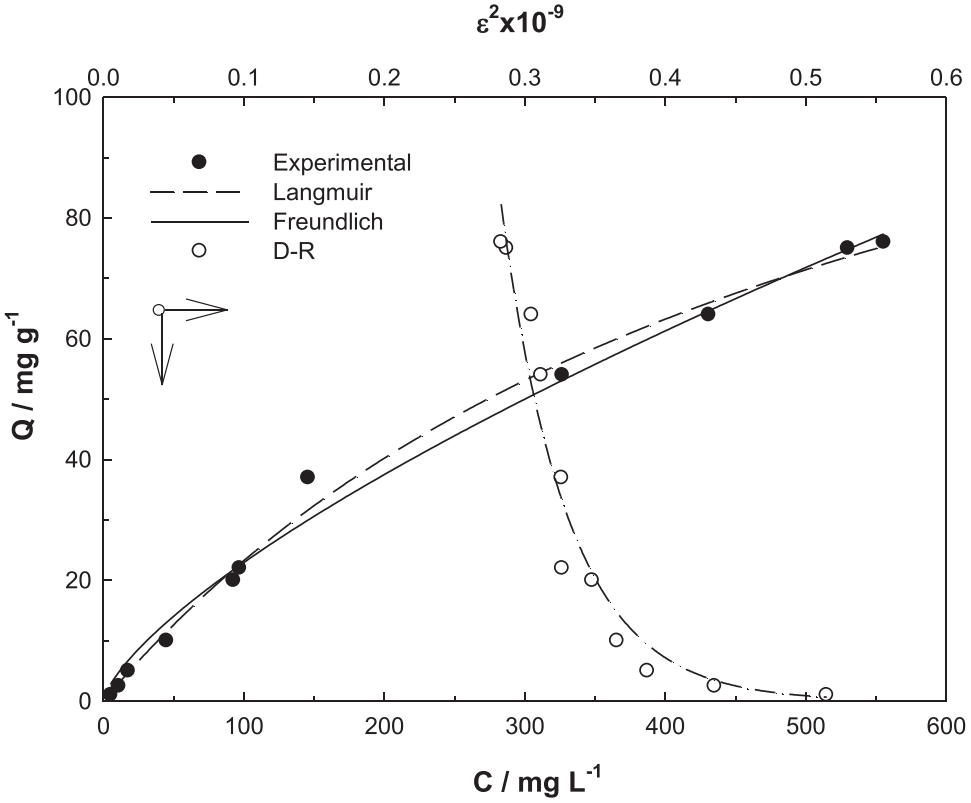

Fig. 6. Compatibility of biosorption isotherms of CA with Langmuir, Freundlich, D-R models {$[CA]_0$:10–1000 mg L^{-1}, biosorbent dosage: 100 mg, V: 10 mL, natural pH: 8.9, contact time:24 h, temperature: 25 °C}.

Table 2
The biosorption kinetics and their parameters.

Kinetic models	Parameters	Value	
PFO	Q_t: the biosorbed amount at the time	Q_t / mg g^{-1}	51.8
$Q_t = Q_e(1 - e^{-k_1 t})$	Q_e: the biosorbed amount at equilibrium	Q_e / mg g^{-1}	46.6
$H_1 = k_1$	t: time	k_1 x10^3/ mg^{-1} g min^{-1}	10.6
	k_1: the rate constant of the PFO		
	H_1: initial biosorption rate for PFO	$H_1 \times 10^3$/mg g^{-1} min^{-1}	493
		R^2	0.808
PSO	k_2: the rate constant of the PSO model	Q_t / mg g^{-1}	51.8
$\frac{t}{Q_t} = \frac{1}{k_2 Q_e^2} + \frac{t}{Q_t}$	H_2: initial biosorption rate for PSO	Q_e / mg g^{-1}	52.3
$H_2 = k_2 Q_t^2$		k_2 x10^3/ mg^{-1} g min^{-1}	0.289
		$H_2 \times 10^3$/mg g^{-1} min^{-1}	790
		R^2	0.881
IPD	k_i: the rate constant of the IPD	k_i x10^3/mg g^{-1} $min^{-0.5}$	7216
$Q_t = k_i t^{0.5}$		R^2	0.985

equilibrium is established between the liquid and solid phases. The PSO kinetic model is applied in chemical adsorption processes that generate covalent forces through the sharing or exchange of electrons between the biosorbent and the adsorbate [30].

The compatibility of the experimental studies with the kinetic models is given in Fig. 7. and the parameters derived from the models are given in Table 2. As seen in Fig. 7, the adsorption of CA dye molecules on the biosorbent reached equilibrium in 240 min. When the regression coefficient (R^2) obtained from the graphs of the PFO and the PSO models and the amount of dye adsorbed at equilibrium are compared, it is seen that the adsorption is more compatible with the PSO model (R^2: 0.882). In addition, the closeness of the theoretically calculated Q_t and experimental Q_e values indicates the fit with the PSO model. According to the obtained data, it was concluded that the adsorption process was chemically realized. In the IPD model, if the plot on the Q-$t^{0,5}$ graph is linear and passes through the origin, only intraparticle diffusion takes place. In multicollinearity, the faster and sharper first line occurs as a result of either outer surface adsorption or rapid boundary layer diffusion at the outer level. The second line represents the dye molecules dispersed in the pores of the biosorbent. This shows that intraparticle diffusion controls the rate and is the rate-limiting step [30]. Adsorption kinetics is explained by the PSO model and the IPD models.

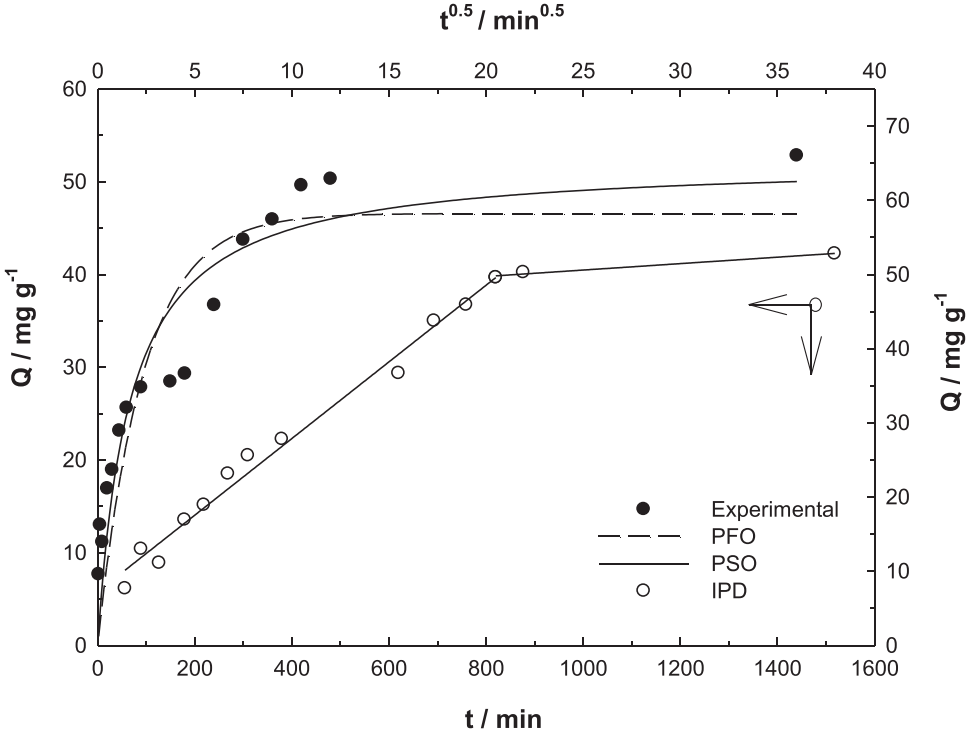

Fig. 7. Compatibility of biosorption kinetics of CA with PFO, PSO, IPD models {$[CA]_0$:500 mg L^{-1}, biosorbent dosage: 100 mg, V: 10 mL, natural pH: 8.9, contact time:10–1440 min, temperature: 25 °C}.

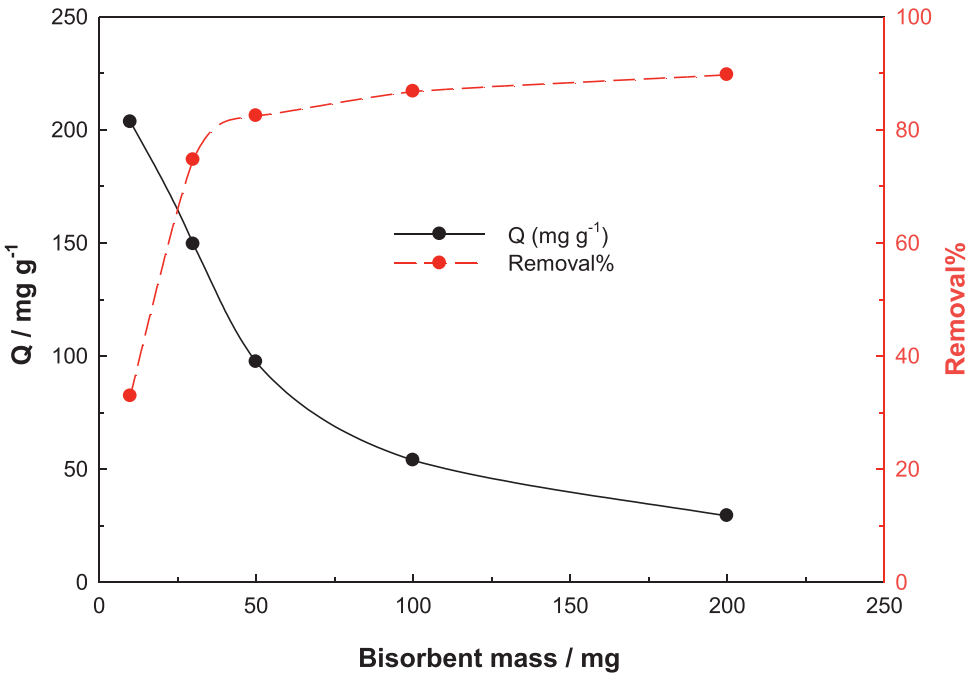

Fig. 8. The effect of the amount of biosorbent on the biosorption of CA dye on MS biosorbent {$[CA]_0$:500 mg L^{-1}, biosorbent dosage: 10, 30, 50, 100 and 200 mg, V: 10 mL, natural pH: 8.9, contact time:24 h, temperature: 25 °C}.

3.7. Effect of biosorbent dosage

The effective use of the amount of biosorbent is an important parameter for determining the biosorption capacity. Studies were conducted to investigate the adsorption of CA dye to MS biosorbent, at an initial concentration of mg L^{-1}, at a dosage of 10–200 mg biosorbent. As seen in Fig. 8, a decrease in the biosorption capacity was detected with the increase in the biosorbent dose. While the amount of CA dye remains constant, the amount of dye to be adsorbed per unit mass decreases with the increase in the amount of biosorbent. The decrease in biosorption capacity with increasing biosorbent dose can be attributed to the unsaturation of active sites on the biosorbent surface during the biosorption reaction.

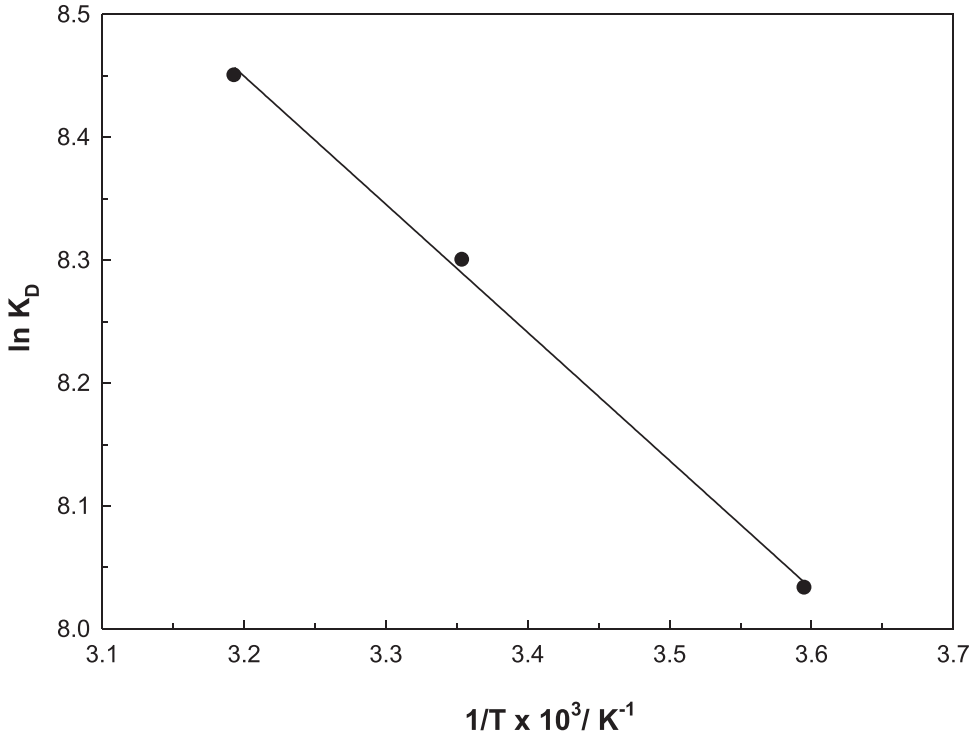

Fig. 9. Effect of temperature on the biosorption of CA dye on MS biosorbent {$[CA]_0$:500 mg L^{-1}, biosorbent dosage: 100 mg, V: 10 mL, natural pH: 8.9, contact time:24 h, temperature: 5 °C, 25 °C and 40 °C}.

3.8. Biosorption thermodynamics

Thermodynamic parameters such as enthalpy change (ΔH^0), free Gibbs energy (ΔG^0), and adsorption entropy (ΔS^0) were calculated to determine the biosorption mechanism and structure of CA to the biosorbent surface. It was studied at an initial concentration of 500 mg L^{-1}, at a dose of 100 mg of biosorbent, in an 8.9 pH environment, for 24 h and at different temperatures such as 5 °C, 20 °C and 40 °C. During the adsorption process, thermodynamic parameters such as ΔH^0, ΔG^0 and ΔS^0 were calculated using the following equations [35,36]. ΔG^0 was determined using Eq. (4).

$$\Delta G^{\circ} = -RTln(K_d) \tag{4}$$

where R (8314 J mol^{-1} K^{-1}) is the ideal gas constant, T (K) is the absolute temperature, and Kd is the distribution coefficient. The dispersion coefficient, which reveals the affinity of the biosorbent surface, is calculated by Eq. (5).

$$K_d = \frac{Q}{C_e} \tag{5}$$

ΔH^0 and ΔS^0 parameters were found using the Van't Hoff Eq. (6).

$$lnK_D = \frac{\Delta S^{\circ}}{R} - \frac{\Delta H^{\circ}}{RT} \tag{6}$$

ΔH^0, ΔG^0 and ΔS^0 were determined using the slope and intercept values of the lnK_D-1/T plot (Fig. 9) [37]. The biosorption enthalpy value was found to be 8.67 kJ mol^{-1}. A positive value indicates that the biosorption process is endothermic. The magnitude of the enthalpy values determines the biosorption mechanism. If the ΔH^0 values are less than 20 kJ mol^{-1}, it indicates that biosorption is physical, such as van der Waals interactions, and if it is between 20 and 80 kJ mol^{-1}, there are electrostatic forces between the dye and the biosorbent [38]. According to the ΔH^0 value obtained, it can be said that the dye molecules are adsorbed by the biosorbent with van der Waals interactions. The positive ΔS^0 (98.1 J mol^{-1} K^{-1}) value found indicates that the irregularity and randomness at the solid-liquid interface increase during biosorption. The ΔG^0 value was calculated as −18.6 kJ mol^{-1}, −20.6 kJ mol^{-1} and −22.0 kJ mol^{-1} at 5 °C, 25 °C and 40 °C, respectively. The increase in ΔG^0 negative values with increasing temperature showed that biosorption was spontaneous and irreversible [39].

3.9. Recovery

The reusability of the biosorbent after the biosorption process is extremely important in terms of being economical and environmentally friendly. Therefore, 5 times desorption experiment was carried out using HCl, ethanol, and methanol solutions with 0,1 mol L^{-1} concentration to recover the CA dye biosorbed on the MS biosorbent surface. The concentration of CA dye recovered after each desorption process was determined by spectrophotometric measurements. Obtained recovery percentages are given in Fig. 10. In Fig. 10, it is seen that the highest recovery is achieved with ethyl alcohol (47.3%) and the lowest recovery is with HCl (23.3%).

3.10. Theoretical prediction of the power of the adsorption

Chemical Reactivity descriptors and electronic structure rules introduced via Conceptual Density Functional Theoretical developments are quite useful in the explaining of the adsorption characteristics of matters [40–46]. One of the old and chemical Reactivity parameters used for this aim of the chemical hardness [47]. This parameter having many applications in the literature is the reported as the resistance against the electron cloud polarization of matters in gas phase. Hard and Soft Acid-Base Principle of Pearson [48] provides important hints about electrostatcic and covalent interactions between chemical species. HSAB Principle states

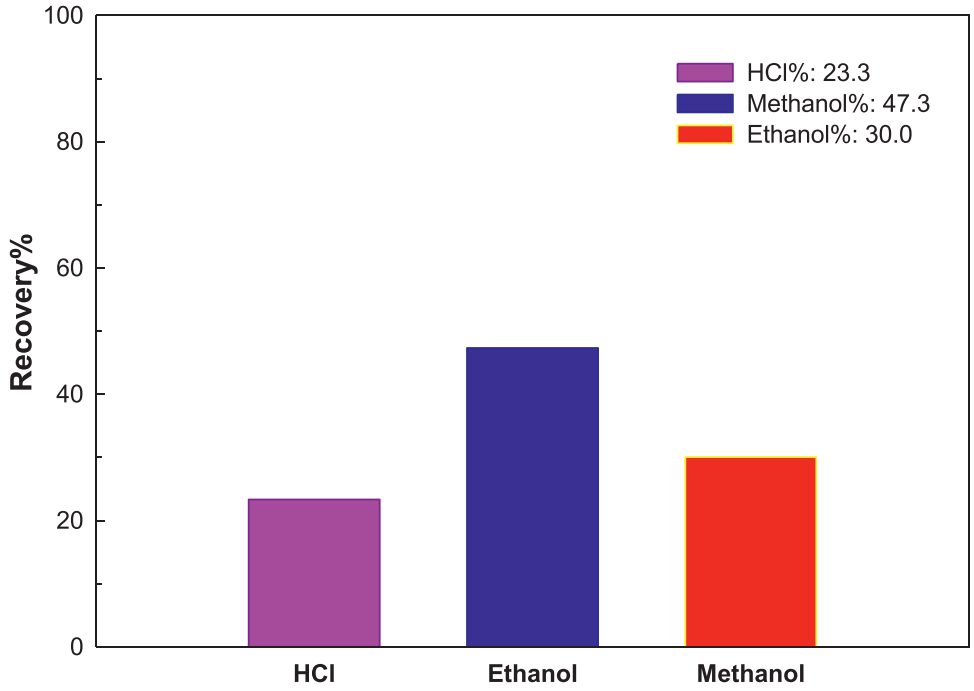

Fig. 10. The effect of recovery on MS biosorbent {$[CA]_0$: 500 mg L^{-1}, biosorbent dosage: 100 mg, V: 10 mL, natural pH: 8.9, contact time: 24 h, temperature: 25 °C}.

that "hard acids prefer the binding to hard bases and soft acids prefer the binding to soft bases." The main reason of the this explanation is that hard-hard and soft-soft interactions are mainly electrostatic and covalent, respectively. The performance in the removing of carminic acid of *Prunus mahaleb* Shell can be easily explained considering HSAB Principle. In a theoretical study, Sun and coworkers [49] calculated the energy difference between HOMO and LUMO orbitals of carminic acid as: 2,94 eV. The calculations were made via DFT using B3LYP functional with a 6-31G(d) basis set. In the Conceptual DFT, chemical hardness (η) is calculated as [50]

$$\eta = I - A$$

In the equation, I and A are ground state ionization energy and electron affinity of the chemical system, respectively. Koopmans [51] proposed the following relations based on the frontier orbital energy levels to compute I and A of molecules.

$$I = -E_{HOMO}$$

$$A = -E_{LUMO}$$

From the given informations, we can say that chemical hardness value of carminic acid is approximately 2.94 eV. From this date, it can be said that covalent interactions are dominant between carminic acid and the chemicals in the structure of *Prunus mahaleb* Shell. Most probably, carminic acid interacts powerful with hydroxycinnamic acids and anthocyanins with close hardness values to that of carminic acid.

4. Conclusion

As a result of the study, it was determined that MS biosorbent is an effective biosorbent for CA dye removal. In order to determine the optimum conditions of this biosorption process, different operating parameters such as pH, initial dye concentration, amount of biosorbent, temperature, contact time were investigated. As a result of the experimental data obtained, it was determined that the CA dye biosorption to the MS biosorbent was more suitable for the Langmuir isotherm and the maximum biosorption capacity of the monolayer was calculated as 148 mg g^{-1}. The E_{DR}:4.89 kJ mol^{-1} determined according to the D-R isotherm showed that the biosorption proceeded physically. Kinetic studies have determined that biosorption follows PSO and IPD kinetic models. According to thermodynamic calculations, the biosorption process is endothermic and spontaneous, and it has been concluded that there is an increase in disorder at the solid-solution interface during biosorption. The comparison of the maximum biosorption capacity of MS biosorbent with other sorbents used in CA dye removal reported in the literature is given in Table 3. According to these results, it was determined that MS biosorbent is an effective biosorbent for CA dye removal. In addition, due to the fact that it is abundant, low cost and renewable due to being agricultural waste, MS biosorbent can be used as an alternative biosorbent in the removal of dyes in wastewater.

Table 3
Sorption capacities of CA in various sorbents.

Sorbent	Sorption capacity (mg g^{-1})	References
Activated Carbon	4.16	[52]
Carbon nanocomposite	33.5	[7]
Mesoporous Carbon	48.5	[53]
Glass powder	4.04	[6]
Prunus mahaleb shell	148	This study

Declaration of Competing Interest

The authors declare that they have no known competing financial interests or personal relationships that could have appeared to influence the work reported in this paper.

CRediT authorship contribution statement

Zehra Seba Keskin: Supervision, Investigation, Methodology, Formal analysis, Data curation, Validation, Writing – review & editing. **Zeynep Mine Şenol:** Investigation, Formal analysis, Writing –

review & editing. **Savaş Kaya:** Investigation, Formal analysis, Writing – review & editing. **Selçuk Şimşek:** Investigation, Formal analysis.

Data availability

No data was used for the research described in the article.

Acknowledgments

The present study was partly supported by Cumhuriyet University Scientific Research Projects Commission. The authors have declared no conflict of interest.

References

[1] A. Hamzezadeh, Y. Rashtbari, S. Afshin, M. Morovati, M. Vosoughi, Application of low-cost material for adsorption of dye from aqueous solution, Int. J. Environ. Anal. Chem. 102 (2022) 254–269.
[2] Y. Hu, R. Han, Selective and efficient removal of anionic dyes from solution by zirconium (IV) hydroxide-coated magnetic materials, J. Chem. Eng. Data 64 (2019) 791–799.
[3] M.K. Sharma, R.C. Sobti, Rec effect of certain textile dyes in Bacillus subtilis, Mutat. Res./Genet. Toxicol. Environ. Mutagen. 465 (2000) 27–38.
[4] K. Kadirvelu, M. Kavipriya, C. Karthika, M. Radhika, N. Vennilamani, S. Pattabhi, Utilization of various agricultural wastes for activated carbon preparation and application for the removal of dyes and metal ions from aqueous solutions, Bioresour. Technol. 87 (2003) 129–132.
[5] A.R. Rahmani, G. Asgari, M. Farrokhi, Removal of reactive black 5 (RB5) dye from aqueous solution using adsorption onto strongly basic anion exchange resin: equilibrium and kinetic study, Iran. J. Health Environ. 5 (2013) 509–518.
[6] G. Atun, G. Hisarli, Adsorption of carminic acid, a dye onto glass powder, Chem. Eng. J. 95 (2003) 241–249.
[7] M. Abbasi, M.M. Sabzehmeidani, M. Ghaedi, R. Jannesar, A. Shokrollahi, Adsorption performance of calcined copper-aluminum layered double hydroxides/CNT/PVDF composite films toward removal of carminic acid, J. Mol. Liq. 329 (2021) 115558.
[8] Z.H. Dastgerdi, V. Abkhiz, S.S. Meshkat, N. Ghorbani, Preparation of novel magnetic grafted raft agent nanocomposite: application in carmine dye adsorptive removal from waste water, J. Environ. Chem. Eng. 7 (2019) 103109.
[9] M.H. Mahnashi, S.S. Abu-Alrub, M.W. Amer, O.A. Alqarni, Kinetics and thermodynamics of enhanced adsorption of E120 dye using activated carbon, Trop. J. Pharm. Res. 20 (2021) 585–592.
[10] M.T. Sulak, E. Demirbas, M. Kobya, Removal of Astrazon Yellow 7GL from aqueous solutions by adsorption onto wheat bran, Bioresour. Technol. 98 (2007) 2590–2598.
[11] M. Shirmardi, F. Khodarahmi, M. Heidari Farsani, A. Naeimabadi, M. Vosughi Niri, J. Jafari, Application of oxidized multiwall carbon nanotubes as a novel adsorbent for removal of Acid Red 18 dye from aqueous solution, J. North Khorasan Univ. Med. Sci. 4 (2012) 335–346.
[12] M.T. Yagub, T.K. Sen, S. Afroze, H.M. Ang, Dye and its removal from aqueous solution by adsorption: a review, Adv. Colloid Interface Sci. 209 (2014) 172–184.
[13] A. Kali, A. Amar, I. Loulidi, M. Jabri, C. Hadey, H. Lgaz, A.A. Alrashdi, F. Boukhlifi, Characterization and adsorption capacity of four low-cost adsorbents based on coconut, almond, walnut, and peanut shells for copper removal, Biomass Convers. Biorefinery (2022) 1–12.
[14] M. El-Azazy, A.S. El-Shafie, A.A. Issa, M. Al-Sulaiti, J. Al-Yafie, B. Shomarand, K. Al-Saad, Potato peels as an adsorbent for heavy metals from aqueous solutions: eco-structuring of a green adsorbent operating Plackett–Burman design, J. Chem. 2019 (2019) 1–14.
[15] H. Hu, J. Zhang, T. Wang, P. Wang, Adsorption of toxic metal ion in agricultural wastewater by torrefaction biochar from bamboo shoot shell, J. Clean. Prod. 338 (2022) 130558.
[16] Ercisli S, E. Orhan, Fatty acid composition of seeds of yellow, red, and black colored Prunus mahaleb fruits in Turkey, Chem. Nat. Compd. 44 (2008) 87–89.
[17] M. Worm, B.M. Henz, Novel unconventional therapeutic approaches to atopic eczema, Dermatology 201 (2000) 191–195.
[18] G.X. Li, Z.Q. Liu, D. Wu, Carminic acid: an antioxidant to protect erythrocytes and DNA against radical-induced oxidation, J. Phys. Org. Chem. 22 (2009) 883–887.
[19] Y.O. Al-Ghamdi, M. Jabli, R. Soury, S.Ali Khan, A cellulosic fruit derived from Nerium oleander biomaterial: chemical characterization and its valuable use in the biosorption of methylene blue in a batch mode, Polymers (Basel) 12 (2020) 2539.
[20] M. Yadav, S. Thakore, R. Jadeja, Removal of organic dyes using Fucus vesiculosus seaweed bioadsorbent an ecofriendly approach: equilibrium, kinetics and thermodynamic studies, Environ. Chem. Ecotoxicol. 4 (2022) 67–77.
[21] R.N. Oliveira, M.C. Mancini, F.C.S.D. Oliveira, T.M. Passos, B. Quilty, R.M.D.S.M. Thiré, G.B. McGuinness, FTIR analysis and quantification of phenols and flavonoids of five commercially available plants extracts used in wound healing, Matéria (Rio de Janeiro) 21 (2016) 767–779.
[22] M. Poletto, A.J. Zattera, R.M. Santana, Structural differences between wood species: evidence from chemical composition, FTIR spectroscopy, and thermogravimetric analysis, J. Appl. Polym. Sci. 126 (2012) E337–E344.
[23] H. Yang, R. Yan, H. Chen, D.H. Lee, C. Zheng, Characteristics of hemicellulose, cellulose and lignin pyrolysis, Fuel 86 (2007) 1781–1788.
[24] F. Largo, R. Haounati, S. Akhouairi, H. Ouachtak, R. El Haouti, A. El Guerdaoui, A.A. Addi, Adsorptive removal of both cationic and anionic dyes by using sepiolite clay mineral as adsorbent: experimental and molecular dynamic simulation studies, J. Mol. Liq. 318 (2020) 114247.
[25] Ü.D. Gül, Z.M. Şenol, B.Ertit Taştan, Treatment of the Allura Red food colorant contaminated water by a novel cyanobacterium Desertifilum tharense, Water Sci. Technol. 8 (2022) 279–290.
[26] T.M. Elmorsi, Z.H. Mohamed, W. Shopak, A.M. Ismaiel, Kinetic and equilibrium isotherms studies of adsorption of Pb (II) from water onto natural adsorbent, J. Environ. Prot. 5 (2014) 1667–1681.
[27] Y.S. Ho, G. McKay, A comparison of chemisorption kinetic models applied to pollutant removal on various sorbents, Process Saf. Environ. Prot. 76 (1998) 332–340.
[28] Y.S. Ho, G. McKay, The kinetics of sorption of divalent metal ions onto sphagnum moss peat, Water Res. 34 (2000) 735–742.
[29] A.J. Varma, S.V. Deshpande, J.F. Kennedy, Metal complexation by chitosan and its derivatives: a review, Carbohydr. Polym. 55 (2004) 77–93.
[30] K.W. Jung, T.U. Jeong, M.J. Hwang, K. Kim, K.H. Ahn, Phosphate adsorption ability of biochar/Mg–Al assembled nanocomposites prepared by aluminum-electrode based electro-assisted modification method with MgCl2 as electrolyte, Bioresour. Technol. 198 (2015) 603–610.
[31] I. Langmuir, The constitution and fundamental properties of solids and liquids. Part I. Solids, J. Am. Chem. Soc. 38 (1916) 2221–2295.
[32] H.M.F. Freundlich, Over the adsorption in solution, J. Phys. Chem. 57 (1906) 1100–1107.
[33] M.M. Dubinin, E.D. Zaverina, L.V. Radushkevich, Sorption and structure of active carbons. I. Adsorption of organic vapors, Zh. Fiz. Khim. 21 (1947) 151–162.
[34] F. Gündüz, B. Bayrak, Biosorption of malachite green from an aqueous solution using pomegranate peel: equilibrium modelling, kinetic and thermodynamic studies, J. Mol. Liq. 243 (2017) 790–798.
[35] Z.M. Şenol, Z.S. Keskin, A. Özer, S. Şimşek, Application of kaolinite-based composite as an adsorbent for removal of uranyl ions from aqueous solution: kinetics and equilibrium study, J. Radioanal. Nucl. Chem. 331 (2022) 403–414.
[36] G.K. Cheruiyot, W.C. Wanyonyi, J. J.Kiplimo, E.N. Maina, Adsorption of toxic crystal violet dye using coffee husks: equilibrium, kinetics and thermodynamics studies, Sci. Afr. 5 (2019) e00116.
[37] G. Li, Y. Du, Y. Tao, H. Deng, X. Luo, J. Yang, Iron (II) cross-linked chitin-based gel beads: preparation, magnetic property and adsorption of methyl orange, Carbohydr. Polym. 82 (2010) 706–713.
[38] G.R. Mahdavinia, F. Bazmizeynabad, B. Seyyedi, Kappa-Carrageenan beads as new adsorbent to remove crystal violet dye from water: adsorption kinetics and isotherm, Desalin. Water Treat. 53 (2015) 2529–2539.
[39] Z.M. Şenol, A chitosan-based composite for adsorption of uranyl ions; mechanism, isothems, kinetics and thermodynamics, Int. J. Biol. Macromol. 183 (2021) 1640–1648.
[40] P. Vennila, M. Govindaraju, G. Venkatesh, C. Kamal, Y.S. Mary, C.Y. Panicker, S.J. Armaković, A complete computational and spectroscopic study of 2-bromo-1, 4-dichlorobenzene—a frequently used benzene derivative, J. Mol. Struct. 1151 (2018) 245–255.
[41] J.S. Al-Otaibi, M. Shabeer, Y.S. Mary, Y.S. Mary, R. Thomas, Adsorption of a thione derivative on carbon, AlN, and BN nanotubes: a detailed DFT and MD investigation, J. Mol. Model. 28 (2022) 1–14.
[42] Y.S. Mary, V.S. Kumar, Y.S. Mary, R. KS, R. Thomas, Detailed quantum mechanical studies on three bioactive benzimidazole derivatives and their Raman enhancement on adsorption over graphene sheets, Polycycl. Aromat. Compd. 42 (2022) 2581–2590.
[43] J.S. Al-Otaibi, Y.S. Mary, Y.S. Mary, R. Thomas, Evidence of cluster formation of pyrrole with mixed silver metal clusters, Agx-My (x= 4, 5, y= 2/1 and M= Au/Ni/Cu) using DFT/SERS analysis, Comput. Theor. Chem. 1208 (2022) 113569.
[44] J.S. Al-Otaibi, Y.S. Mary, Y.S. Mary, R. Thomas, Evidence of cluster formation of croconic acid with Ag, Au and Cu cages, enhancement of electronic properties and Raman activity, Spectrochim. Acta A 264 (2022) 120233.
[45] U. Bhattacharyya, T. Pooventhiran, R. Thomas, Adsorption of the drug bempedoic acid over different 2D/3D nanosurfaces and enhancement of Raman activity enabling ultrasensitive detection: first principle analysis, Spectrochim. Acta A 254 (2021) 119630.
[46] A. Alsalme, T. Pooventhiran, N. Al-Zaqri, D.J. Rao, R. Thomas, Structural, physico-chemical landscapes, ground state and excited state properties in different solvent atmosphere of Avapritinib and its ultrasensitive detection using SERS/GERS on self-assembly formation with graphene quantum dots, J. Mol. Liq. 322 (2021) 114555.
[47] A. Thakur, S. Kaya, A.S. Abousalem, A. Kumar, Experimental, DFT and MC simulation analysis of Vicia Sativa weed aerial extract as sustainable and eco-benign corrosion inhibitor for mild steel in acidic environment, Sustain. Chem. Pharm. 29 (2022) 100785.
[48] R.G. Pearson, Hard and soft acids and bases, J. Am. Chem. Soc. 85 (1963) 3533–3539.

[49] C. Sun, Y. Li, P. Song, F. Ma, An experimental and theoretical investigation of the electronic structures and photoelectrical properties of ethyl red and carminic acid for DSSC application, Materials (Basel) 9 (2016) 813.
[50] N. Islam, S. Kaya (Eds.), Conceptual density functional theory and its application in the chemical domain, CRC Press, 2018.
[51] T. Koopmans, Über die Zuordnung von Wellenfunktionen und Eigenwerten zu den einzelnen Elektronen eines Atoms, physica, 1 (1934) 104–113.
[52] M.H. Mahnashi, S.S. Abu-Alrub, M.W. Amer, A.O. Alqarni, Kinetics and thermodynamics of enhanced adsorption of E120 dye using activated carbon, Trop. J. Pharm. Res. 20 (2021) 585–592.
[53] M. Misriyani, T. Setianingsih, D. Darjito, Effect of carbonization time of mesoporous carbon in the dyes adsorption: Rhodamine B, methylene blue and carmine. IJFAC indones, J. Fundam. Appl. Chem. 5 (2020) 1–6.